Mineralogy and Petrology (2006) 88: 243–267
DOI 10.1007/s00710-006-0157-1

Mineralogy and Petrology

Printed in Austria

Franciscan eclogite revisited: Reevaluation of the *P–T* evolution of tectonic blocks from Tiburon Peninsula, California, U.S.A.

T. Tsujimori[1], **K. Matsumoto**[2], **J. Wakabayashi**[3], and **J. G. Liou**[1]

[1] Department of Geological and Environmental Sciences, Stanford University, Stanford, California, U.S.A.
[2] Department of Geology and Mineralogy, Graduate School of Science, Kyoto University, Kyoto, Japan
[3] Department of Earth and Environmental Sciences, California State University, Fresno, California, U.S.A.

Received September 10, 2005; accepted March 30, 2006
Published online August 22, 2006;
Editorial handling: A. Proyer

Summary

High-grade blocks in the Franciscan complex at Tiburon, California, record relatively low temperature eclogite-facies metamorphism and blueschist-facies overprinting. The eclogite-facies mineral assemblage contains prograde-zoned garnet + omphacite + epidote ± hornblende (katophoritic and barroisitic Ca–Na amphibole) ± glaucophane + phengite (~3.5 Si p.f.u.) ± paragonite + rutile + quartz. The blueschist-facies mineral assemblage contains chlorite + titanite + glaucophane + epidote ± albite ± phengite (~3.3 Si p.f.u.). Albite is not stable in the eclogite stage. New calculations based on garnet-omphacite-phengite thermobarometry and THERMOCALC average-*P–T* calculations yield peak eclogite-facies *P–T* conditions of $P = 2.2$–2.5 GPa and $T = 550$–620 °C; porphyroclastic omphacite with inclusions of garnet and paragonite yields an average-*P–T* of 1.8 ± 0.2 GPa at 490 ± 70 °C for the pre-peak stage. The inferred counterclockwise hairpin *P–T* trajectory suggests prograde eclogitization of a relatively ''cold'' subducting slab, and subsequent exhumation and blueschist-facies recrystallization by a decreasing geotherm. Although an epidote-garnet amphibolitic assemblage is ubiquitous in some blocks, *P–T* pseudosection analyses imply that the epidote-garnet amphibolitic assemblage is stable during prograde eclogite-facies metamorphism. Available geochronologic data combined with our new insight for the maximum pressure suggest an average exhumation rate of ~5 km/Ma, as rapid as those of some ultrahigh pressure metamorphic terranes.

Introduction

The Franciscan Complex of the California Coast Ranges is the one of the classic localities of high-pressure (HP) and low-temperature (LT) eclogite (cf. *Schliestedt*, 1990). Franciscan eclogite (*sensu lato*) occurs commonly as meter-scale tectonic blocks in a serpentinite- or shale-matrix mélange (e.g., *Coleman* et al., 1965; *Coleman* and *Lanphere*, 1971; *Brown* and *Bradshaw*, 1979; *Moore*, 1984; *Moore* and *Blake*, 1989; *Wakabayashi*, 1990, 1999; *Cloos*, 1986; *Oh* and *Liou*, 1990; *Krogh* et al., 1994; *Tsujimori* et al., in press). Although the geochronologic aspects of Franciscan eclogites have been recently updated (e.g., *Catlos* and *Sorensen*, 2003; *Anczkiewicz* et al., 2004), metamorphic petrology has not been reevaluated in almost a decade. What is the pressure maximum of Franciscan eclogite? How deeply were Franciscan eclogites subducted? It has been considered that Franciscan eclogite was formed within the albite stability field – below the univariant reaction albite = jadeite + quartz (e.g., *Moore*, 1984; *Oh* and *Liou*, 1990; *Wakabayashi*, 1990). It is true that some Franciscan eclogites contain minor albite. However, as we concluded in this paper, the eclogite-facies metamorphism of Franciscan high-grade blocks experienced much higher pressure, probably just below the univariant reaction paragonite = kyanite + jadeite. In this paper, we describe petrologic characteristics of three eclogitic rocks from Ring Mountain of the Tiburon Peninsula in the San Francisco Bay region, and then we reinterpret the *P–T* path of these Franciscan eclogites.

Mineral abbreviations are after *Kretz* (1983); we also use phengite (Phe) throughout this paper. 'Hornblende (Hbl)' is used to describe Ca–Na amphibole with dominantly katophoritic and barroisitic (*Leake* et al., 1997) composition.

Geological background

Franciscan high-grade blocks

The highest-grade metamorphic rocks of the Franciscan complex are coarse-grained blueschists, eclogites, and amphibolites that occur almost entirely as tectonic blocks in shale or serpentinite-matrix mélanges. These tectonic blocks are called "high-grade blocks" (*Coleman* and *Lanphere*, 1971). Although high-grade blocks make up much less than one percent of Franciscan metamorphic rocks, they are widely distributed, occurring at hundreds of localities along the length of the exhumed subduction complex (*Coleman* and *Lanphere*, 1971). Many, if not most, high-grade blueschist and eclogite blocks have relics of earlier amphibolite-grade metamorphic assemblages (*Moore* and *Blake*, 1989; *Wakabayashi*, 1990). The *P–T* conditions of high-grade block metamorphism appear to have evolved progressively from higher to lower geothermal gradients, defining a counterclockwise *P–T* path (*P* on positive y-axis) (*Wakabayashi*, 1990; *Oh* and *Liou*, 1990; *Krogh* et al., 1994). High-grade blocks are predominantly metabasites with minor metacherts (*Blake* et al., 1988; *Coleman* and *Lanphere*, 1971). Many high-grade blocks are partly encased in "rinds" composed of minerals such as actinolite, chlorite, talc, and phengite: these rinds apparently formed by metasomatic reactions between the block and surrounding ultramafic rocks (e.g., *Coleman* and *Lanphere*, 1971; *Moore*, 1984; *Catlos* and *Sorensen*, 2003).

The high-grade blocks are the oldest metamorphic rocks in the Franciscan, and their age of high-temperature metamorphism is 153–169 Ma, based on $^{40}Ar/^{39}Ar$ hornblende and Lu–Hf garnet ages (*Ross* and *Sharp*, 1988; *Catlos* and *Sorensen*, 2003; *Anczkiewicz* et al., 2004). The age of blueschist-facies metamorphism of the blocks ranges from 138 to 159 Ma (*Wakabayashi*, 1999). The age of high-temperature metamorphism in the high-grade blocks is slightly younger than the crystallization age of the 165–172 Ma Coast Range Ophiolite and associated rocks (*Mattinson* and *Hopson*, 1992; *Hanan* et al., 1992; *Hopson* et al., 1996; *Shervais* et al., 2005).

The geochemistry of high-grade block metabasites suggests a nascent arc origin for the protolith, similar to the unmetamorphosed basalts of the Coast

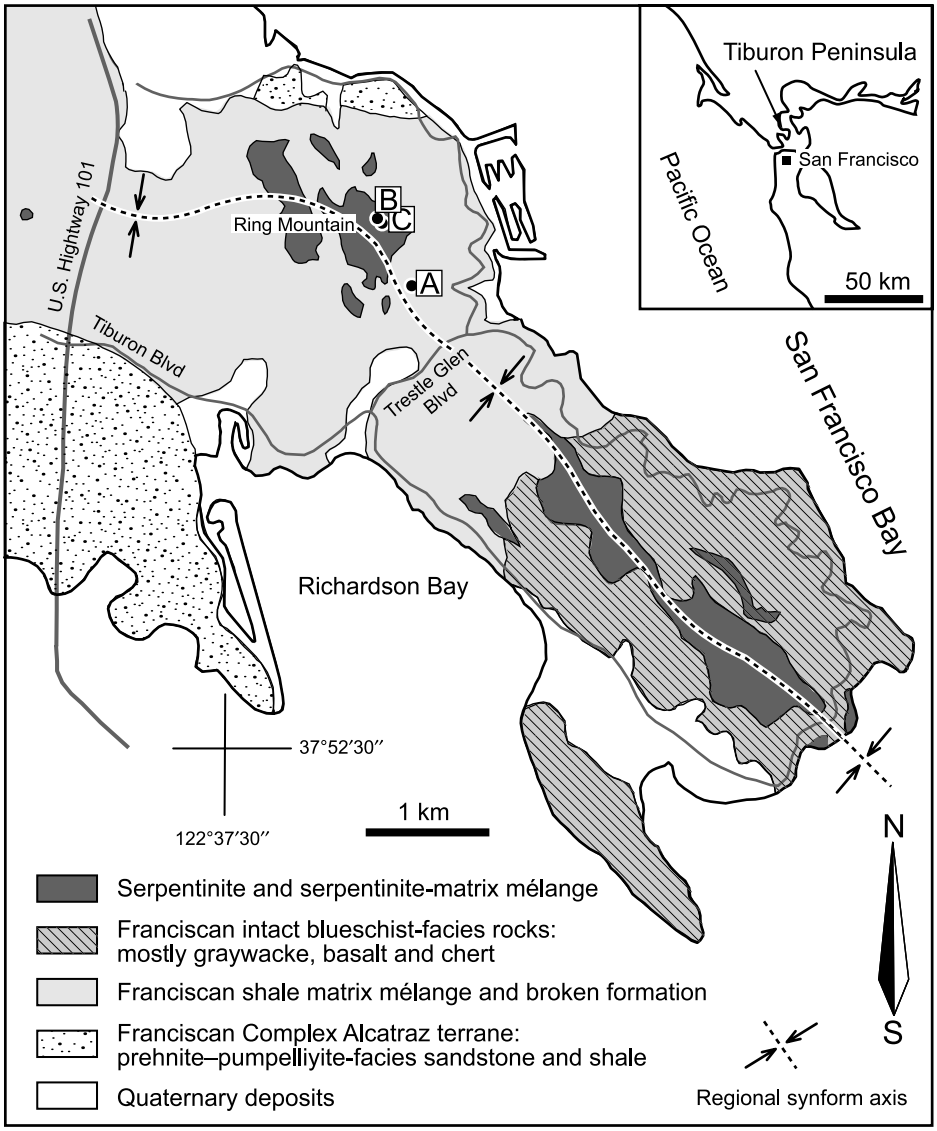

Fig. 1. Simplified geologic map of the Tiburon Peninsula (after *Wakabayashi*, 1990). Labelled square represents sample localities

Range ophiolite that structurally overlies the Franciscan (*Saha* et al., 2005). The nascent arc geochemistry of the high-grade blocks contrasts with the MORB or OIB geochemistry of younger, lower grade metabasites of the Franciscan (*Shervais*, 1990).

The age of the high-grade blocks, their geologic setting and their *P–T* evolution suggests that the high-grade blocks were initially metamorphosed at the inception of subduction beneath the young, hot Coast Range ophiolite in a setting analogous to the metamorphic soles that are found beneath many ophiolites (*Wakabayashi*, 1990). The progressive overprinting of assemblages by lower geothermal gradients reflects subduction refrigeration after the tectonic underplating of the high-grade blocks (*Wakabayashi*, 1990). Lu–Hf garnet ages show systematically older ages for higher peak metamorphic temperatures, and the fairly large spread of ages (153–169 Ma) has been interpreted as evidence for slow initial subduction (*Ancziewicz* et al., 2004).

Ring mountain

Franciscan eclogites (*sensu lato*) analyzed in this study were collected from a serpentinite-matrix mélange from the Ring Mountain of the Tiburon Peninsula in the San Francisco Bay region (Fig. 1). This mélange is the structurally highest of the series of Franciscan nappes in the region (*Wakabayashi*, 1992). A variety of block types occur at Ring Mountain, including garnet amphibolites, epidote amphibolites, eclogites, and blueschists, and corresponding peak metamorphic *P–T* conditions also vary widely from block to block. In addition to the region-wide geochronologic data on high-grade blocks reviewed above, previous detailed geochronologic data have been obtained specifically from high-grade blocks at Ring Mountain. Spot $^{40}Ar/^{39}Ar$ dates on phengites from garnet amphibolite and eclogite (range 151.6 ± 4.1 to 157.5 ± 1.8 Ma), block rind (range 141.0 ± 1.7 to 160.6 ± 3.3 Ma), and a phengite chlorite vein (range 150.2 ± 1.1 to 160.3 ± 5.2 Ma), represent a total of 37 analyses (*Catlos* and *Sorensen*, 2003). A Lu–Hf garnet age of 153 ± 0.4 Ma was obtained from a garnet amphibolite (*Ancziewicz* et al., 2004).

Petrography

Three samples from the Ring Mountain are investigated in this study. Their lithologic and petrographic features are described below:

Sample A

This sample is the same block ($2 \times 3 \times 1.5$ m) that was sampled and labeled ''TIBB'' in *Wakabayashi* (1990) and *Saha* et al. (2005) and ''PG23'' in *Anczkiewicz* et al. (2004); it is a medium-grained garnet amphibolite with a late eclogitic mineral assemblage and blueschist-facies overprinting. The block shows rare tight to isoclinal folds ($F_1{}^A$); a penetrative schistosity $S_1{}^A$ along the axial planes of $F_0{}^A$ has overprinted earlier deformational structures (Fig. 2a). Minor post-$S_1{}^A$ deformation occurs as later crenulations and veins. Sample A consists mainly of hornblende

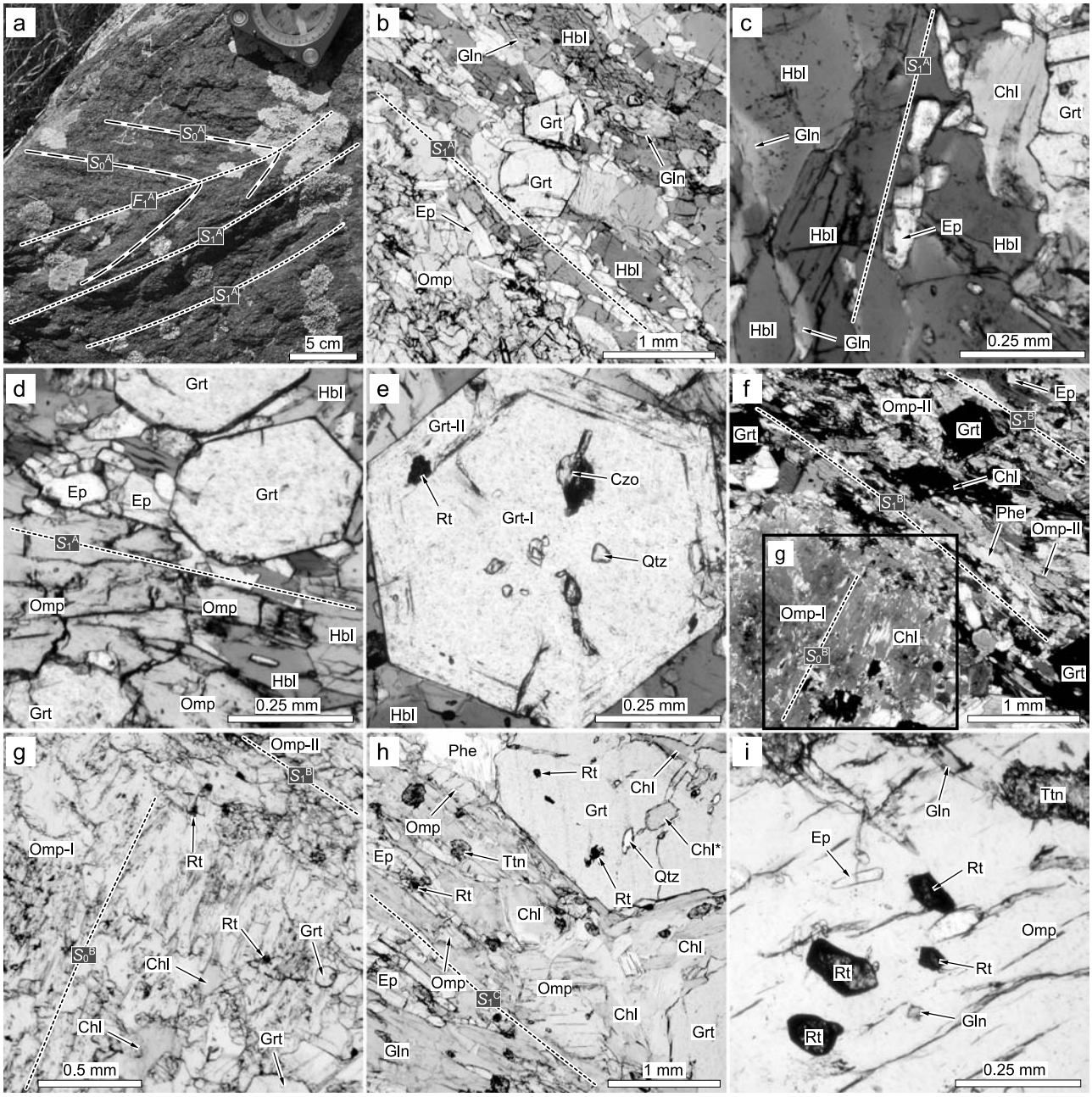

Fig. 2. Photomicrographs showing meso- and microtextures of the investigated samples. (**a**) Isoclinal folds in sample A showing the transition from $S_0{}^A$ to $S_1{}^A$. (**b**) Hornblende-rich foliated matrix of sample A [plane polarized light = PPL]. (**c**) Retrograde glaucophane overgrown on hornblende of sample A [PPL]. Note that porphyroblastic garnet is partly replaced by retrograde chlorite. (**d**) Omphacite coexisting with both garnet and hornblende of sample A [PPL]. (**e**) Garnet porphyroblast of sample A [PPL]. (**f**) Well-deformed matrix of sample B showing the transition from $S_0{}^B$ to $S_1{}^B$; $S_0{}^b$ preserved as internal fabric of omphacite porphyroclast [crossed-polarized light]. (e) Enlarged view of omphacite porphyroclast in f [PPL]. (**h**) Retrograde matrix of sample C [PPL]. (**i**) Mineral inclusions within relict omphacite of sample C. Titanite is a secondary phase replacing rutile along a crack

(56 vol.%), epidote (19 vol.%), chloritized garnet (13 vol.%), omphacite (11 vol.%), with minor rutile, titanite, phengite and quartz (Fig. 2b). Apatite, zircon and iron sulfide are accessories. Green pleochroic hornblende (<2 mm) defines the schistosity $S_1{}^A$; retrograde glaucophane overgrows the margins and fills internal cracks of hornblende (Fig. 2c). Epidote occurs as oriented prisms (<0.5 mm) roughly parallel to $S_1{}^A$ (Fig. 2b, c). Garnet is subhedral to euhedral (0.3–1.5 mm) and partly chloritized along margins and internal cracks (Fig. 2c–e). Some garnet porphyroblasts are subdivided texturally into core (garnet-I) and rim (garnet-II) (Fig. 2e). Garnet-I contains mineral inclusions of epidote, quartz and rare rutile, whereas garnet-II contains rutile and rare phengite; rutile needles are common in garnet-II. Omphacite occurs as aggregates of prismatic or irregular-shaped crystals (~0.5 mm); some omphacites are in direct contact with garnet-II and hornblende (Fig. 2d). Omphacite contains inclusions of epidote, quartz and rare rutile and prograde eclogite-facies glaucophane. Titanite replacing rutile is ubiquitous in the matrix.

Petrographic relations indicate at least three stages of metamorphic recrystallization: a garnet-epidote amphibolitic stage ($M_0{}^A$), a peak eclogite-facies stage ($M_1{}^A$), and a later blueschist-facies stage ($M_2{}^A$). The $M_0{}^A$ is characterized by the assemblage Hbl + Ep + Grt-I + Rt + Qtz. The assemblage Grt-II + Omp + Ep + Hbl + Gln + Rt ± Phe + Qtz characterizes the $M_1{}^A$ stage; we interpret that both hornblende and prograde glaucophane are stable during the peak eclogite-facies stage. The $M_2{}^A$ assemblage Chl + Gln + Ttn overprints both $M_0{}^A$ and $M_1{}^A$ stage mineral assemblages.

Sample B

This sample was collected from a fragment (1×2×1 m) of a less-retrograded eclogite knocker labeled ''EC'' and ''E-1'' in *Saha* et al. (2005); it is fine-grained schistose eclogite. A penetrative schistosity $S_1{}^B$ is defined by preferred orientation of omphacite and phengite. Sample B consists mainly of omphacite (48 vol.%), epidote (26 vol.%), garnet (21 vol.%), and phengite (3 vol.%), with minor rutile, titanite, chlorite, quartz, and rare glaucophane, hornblende and paragonite. Apatite and iron sulfide are accessories. Most omphacite grains occur as fine-grained prisms (<1 mm in length) parallel to the schistosity $S_1{}^B$ (omphacite-II). Some earlier, coarse-grained omphacite porphyroblasts (2–3 mm) (omphacite-I) with an earlier inclusion fabric $S_0{}^B$ are wrapped by $S_1{}^B$ layers of omphacite-II (Fig. 2f). This textural relation indicates that coarse-grained omphacite-I underwent grain-size reduction by recrystallization during eclogite-facies deformation. Omphacite-I contains inclusions of quartz, rutile, epidote, garnet and rare paragonite; it is partly replaced by secondary chlorite (Fig. 2g). Omphacite-II is also replaced by chlorite. Matrix garnet is subhedral to euhedral (0.1 to 1 mm); it contains quartz, epidote and rare rutile and prograde glaucophane. Rare hornblende (<0.1 mm) occurs in the matrix. Matrix rutile is commonly replaced by titanite.

Petrographic relations indicate two eclogite-facies deformational phases ($M_{0-1}{}^B$). The $M_{0-1}{}^B$ is characterized by the assemblage Grt + Omp + Ep ± Gln ± Hbl ± Pg + Rt + Phe + Qtz. The overprinting mineral assemblage Chl + Gln + Ttn might be comparable to blueschist-facies retrogression $M_2{}^A$.

Sample C

This sample was collected as sub-rounded boulder float (20×25×30 cm) in a creek; it is medium-grained garnet blueschist with relict eclogitic omphacite. A penetrative schistosity $S_1{}^C$ is defined by glaucophane and phengite. Sample C consists mainly of glaucophane (44 vol.%), chloritized garnet (25 vol.%), omphacite (12 vol.%), epidote (9 vol.%), phengite + chlorite (8 vol.%), with minor titanite, rutile, quartz and albite. Glaucophane occurs as nematoblasts parallel to $S_1{}^C$ (<1 mm) and it contains mineral inclusions of quartz, epidote, and titanite. Glaucophane is commonly associated with secondary chlorite replacing garnet; most glaucophane crystals appear to be retrograded. Garnet is subhedral to euhedral (0.5 to 2.2 mm), and intensely chloritized along margins and internal cracks; it contains rutile, epidote, quartz and rare phengite. Some polycrystaline chlorite inclusions in garnet could be omphacite pseudomorphs (Fig. 2h). Relict omphacite occurs as irregular-shaped crystals (<2 mm) and contains inclusions of rutile, prograde glaucophane, epidote and rare quartz (Fig. 2i); omphacite is partly replaced by chlorite. Matrix phengite is closely associated with chlorite and titanite; in some cases those retrograde phengites replace garnet rims. Minor albite occurs as secondary veins filling cracks of garnet.

Petrographic relations indicate a peak eclogite-facies stage ($M_1{}^C$) characterized by the relict assemblage Grt + Omp + Ep + Gln ± Phe + Rt + Qtz; hornblende has not yet been confirmed in this sample. The later blueschist-facies stage ($M_2{}^C$) is characterized by the assemblage Chl + Gln + Ep + Phe + Ttn + Qtz ± Ab.

Mineral compositions

Electron microprobe analysis was performed with a JEOL JXA-8900R at Okayama University of Science. Quantitative analyses were performed with 15 kV accelerating voltage, 12 nA beam current and 3–5 μm beam size. Natural and synthetic silicates and oxides were used as standards for calibration. The CITZAF method (*Armstrong*, 1988) was employed for matrix corrections. Representative analyses are listed in Table 1. Fe was assumed to be Fe^{2+} unless otherwise noted.

Garnets

Garnets are zoned with spessartine-rich cores; X_{Mg} [$= Mg/(Mg + Fe^{2+})$] increases continuously toward the rim (Fig. 3), but the nature of this trend varies with sample. For example, the lowest X_{Mg} values are sample A (garnet-I: 0.16; garnet-II: 0.18), sample B (0.14), and sample C (0.10). Garnet-I is characterized by the most spessartine-rich compositions: $alm_{51-54}grs_{26-30}prp_{10-14}sps_{5-11}$, with $X_{Mg} = 0.16$–0.21, whereas garnet-II is characterized by a compositional range: $alm_{54-58}grs_{25-28}prp_{13-16}sps_{3-4}$, with $X_{Mg} = 0.14$–0.23. Garnet in sample B is characterized by a wider compositional range: $alm_{54-59}grs_{25-30}prp_{9-16}sps_{1-8}$, with $X_{Mg} = 0.04$–0.22; the highest X_{Mg} rim values are similar to that in garnet-I of sample A. Inclusion garnet within omphacite-I has an intermediate composition with $X_{Mg} = 0.17$. Garnet in sample C is characterized by the most almandine-rich composition: $alm_{59-63}grs_{24-28}prp_{7-13}sps_{2-7}$, with $X_{Mg} = 0.10$–0.17.

Table 1. *Representative microprobe analyses of minerals from eclogitic rocks from Ring Mountain at Tiburon*

Mineral		SiO_2	TiO_2	Al_2O_3	Cr_2O_3	FeO*	MnO	MgO	CaO	Na_2O	K_2O	Total	O =	Si	Ti	Al	Cr	Fe^{3+}	Fe^{2+}	Mn	Mg	Ca	Na	K	Total
Sample A																									
Grit	core	38.6	0.1	21.3	0.0	26.1	1.7	3.5	9.3	0.0	0.0	100.6	*12*	3	0	2	0.00		1.7	0.1	0.4	0.8	0.00	0.00	8.00
Grt	rim	38.7	0.1	21.4	0.0	25.3	1.6	4.1	9.4	0.0	0.0	100.5	*12*	3	0	2	0.00		1.6	0.1	0.5	0.8	0.00	0.00	8.00
Grt-I	core	37.5	0.1	21.2	0.0	24.4	3.9	3.3	9.3	0.0	0.0	99.8	*12*	2.98	0.01	1.98	0.00		1.62	0.26	0.39	0.79	0.01	0.00	8.03
Grt-II	rim	38.3	0.0	21.6	0.0	26.1	1.5	3.7	9.2	0.0	0.0	100.4	*12*	3.00	0.00	1.99	0.00		1.71	0.10	0.44	0.77	0.01	0.00	8.01
Omp		55.2	0.1	9.4	0.0	7.4	0.0	7.3	12.4	7.2	0.0	98.9	*6*	2.00	0.00	0.40	0.00	0.08	0.15	0.00	0.39	0.48	0.50	0.00	4.00
Hbl		44.0	0.6	13.9	0.0	13.6	0.1	10.6	8.8	3.9	0.6	96.3	*23*	6.49	0.07	2.42	0.00	0.44	1.24	0.02	2.33	1.40	1.12	0.12	15.63
Gln	inc. O	56.2	0.0	9.3	0.0	11.0	0.1	11.3	2.6	6.5	0.1	97.0	*23*	7.84	0.00	1.52	0.00	0.26	1.03	0.01	2.34	0.39	1.75	0.01	15.15
Gln		55.8	0.0	9.1	0.0	15.0	0.1	8.3	0.6	7.3	0.0	96.2	*23*	7.93	0.00	1.52	0.00	0.39	1.39	0.01	1.75	0.10	2.02	0.01	15.12
Ep		37.9	0.2	26.1	0.0	8.2	0.2	0.1	23.7	0.0	0.0	96.3	*13*	2.99	0.01	2.43	0.00	0.54		0.01	0.01	2.01	0.00	0.00	8.01
Phe		50.2	0.2	25.2	0.0	3.4	0.0	3.6	0.0	0.3	10.4	93.3	*11*	3.44	0.01	2.04	0.00		0.19	0.00	0.37	0.00	0.05	0.91	7.01
Sample B																									
Grt	core	37.7	0.2	20.8	0.0	26.7	2.0	2.7	9.9	0.0	0.0	100.1	*12*	2.99	0.01	1.95	0.00		1.77	0.14	0.32	0.85	0.00	0.00	8.03
Grt	rim	38.3	0.1	21.5	0.0	25.3	0.5	3.9	10.5	0.0	0.0	100.2	*12*	3.00	0.00	1.98	0.00		1.66	0.04	0.46	0.88	0.00	0.00	8.01
Grt	inc. O	37.5	0.1	20.8	0.0	26.6	1.8	3.0	10.5	0.0	0.0	100.3	*12*	2.97	0.00	1.95	0.00		1.76	0.12	0.35	0.89	0.00	0.00	8.05
Omp-I		54.8	0.0	9.2	0.1	5.7	0.1	8.4	13.7	6.4	0.0	98.3	*6*	1.99	0.00	0.39	0.00	0.07	0.10	0.00	0.45	0.53	0.45	0.00	4.00
Omp-II		55.8	0.0	10.3	0.0	4.3	0.0	8.5	13.7	6.7	0.0	99.3	*6*	2.00	0.00	0.43	0.00	0.04	0.09	0.00	0.45	0.53	0.47	0.00	4.00
Hbl		46.2	0.3	14.8	0.1	14.8	0.0	9.0	6.9	4.5	0.4	97.0	*23*	6.69	0.03	2.53	0.01	0.56	1.23	0.00	1.95	1.06	1.26	0.08	15.40
Gln	inc. G	57.1	0.0	11.2	0.0	12.1	0.0	8.4	0.2	7.2	0.0	96.3	*23*	7.99	0.00	1.84	0.00	0.16	1.26	0.00	1.75	0.03	1.96	0.00	14.99
Ep		37.6	0.1	26.6	0.1	7.9	0.1	0.1	23.6	0.0	0.0	96.0	*13*	2.98	0.01	2.48	0.01	0.52		0.01	0.01	2.00	0.00	0.00	8.01
Pg	inc. O	47.2	0.0	39.8	0.0	0.4	0.0	0.1	0.1	6.9	0.6	95.1	*11*	3.01	0.00	2.99	0.00		0.02	0.00	0.01	0.01	0.86	0.05	6.95
Phe		50.1	0.2	25.8	0.1	2.7	0.0	3.8	0.0	0.3	10.4	93.3	*11*	3.42	0.01	2.08	0.00		0.16	0.00	0.38	0.00	0.04	0.90	7.00
Sample C																									
Grt	core	37.9	0.2	20.8	0.0	28.3	1.7	2.2	9.6	0.0	0.0	100.7	*12*	3.00	0.01	1.94	0.00		1.88	0.11	0.26	0.81	0.00	0.00	8.02
Grt	rim	38.0	0.0	20.9	0.0	27.8	1.0	3.0	9.6	0.0	0.0	100.5	*12*	3.00	0.00	1.95	0.00		1.84	0.07	0.35	0.81	0.00	0.00	8.02
Omp		55.7	0.1	8.8	0.0	7.5	0.1	7.6	13.6	6.8	0.0	100.1	*6*	2.00	0.00	0.37	0.00	0.10	0.13	0.00	0.41	0.52	0.47	0.00	4.00
Gln	inc. O	56.1	0.0	10.1	0.0	12.2	0.0	9.9	1.4	6.7	0.0	96.4	*23*	7.85	0.00	1.66	0.00	0.39	1.03	0.00	2.06	0.21	1.83	0.01	15.04
Gln		56.5	0.0	10.5	0.0	13.0	0.0	8.8	0.9	7.2	0.0	97.0	*23*	7.90	0.00	1.73	0.00	0.23	1.29	0.00	1.84	0.14	1.95	0.00	15.09
Ep		37.8	0.2	27.1	0.0	7.8	0.1	0.1	23.3	0.0	0.0	96.4	*13*	2.98	0.01	2.51	0.00	0.51		0.01	0.02	1.97	0.00	0.00	8.00
Phe		49.1	0.6	28.7	0.0	2.7	0.0	2.6	0.0	1.0	9.4	94.1	*11*	3.31	0.03	2.29	0.00		0.15	0.00	0.26	0.00	0.13	0.81	6.99
Phe	inc. G	51.4	0.1	24.7	0.0	4.5	0.1	3.3	0.0	0.1	10.1	94.2	*11*	3.49	0.00	1.98	0.00		0.26	0.01	0.33	0.00	0.01	0.88	6.96

*FeO** Total Fe as Fe^{2+}. See text for calculation of Fe^{3+}/Fe^{2+} ratio of clinopyroxene
inc. G Inclusion in garnet; *inc. O* inclusion in omphacite

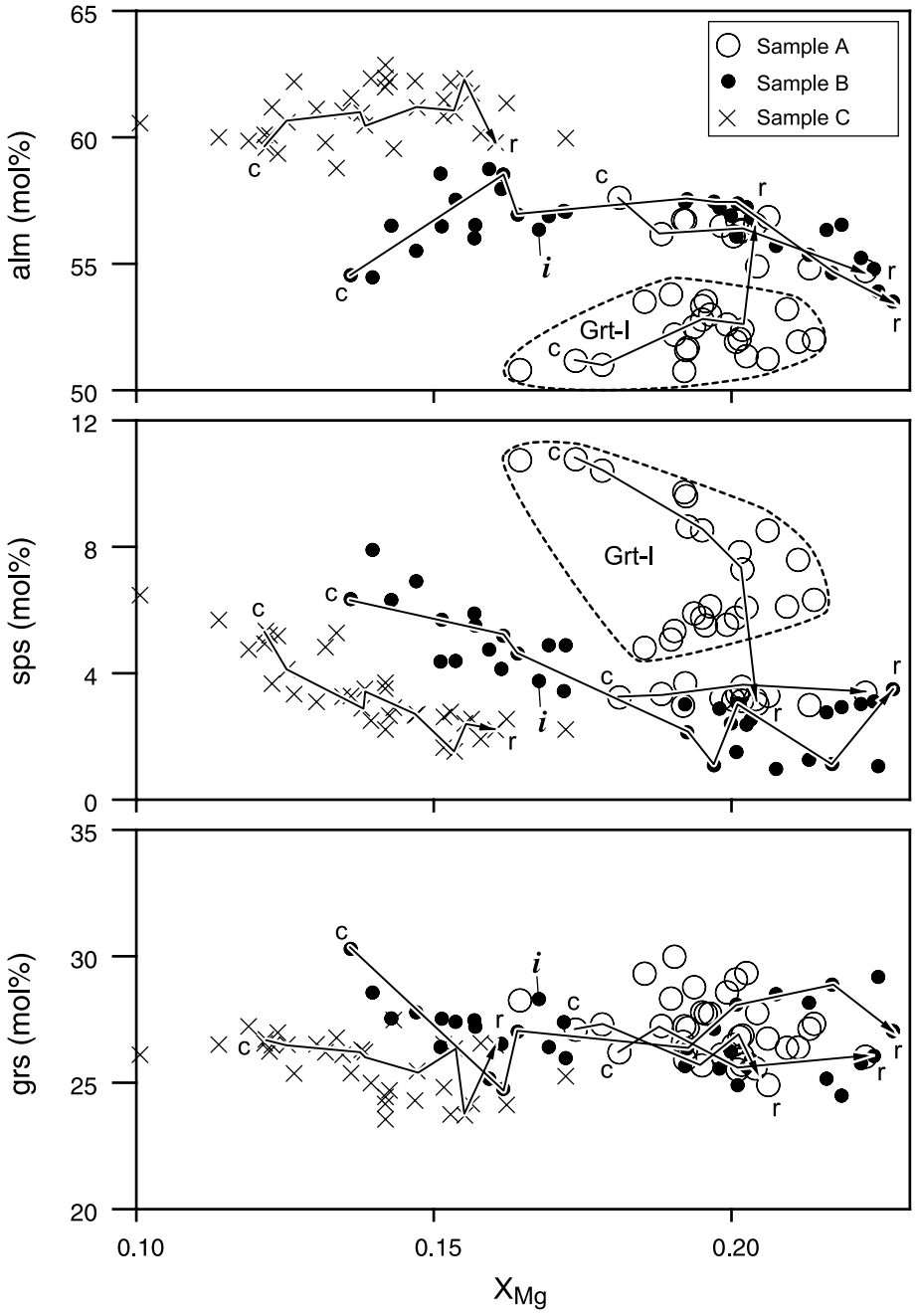

Fig. 3. Compositional trends of garnet in investigated rocks from Tiburon; *alm* almandine [$=100\times Fe/(Fe+Mn+Mg+Ca)$], *sps* spessartine [$=100\times Mn/(Fe+Mn+Mg+Ca)$], and *grs* grossular [$=100\times Ca/(Fe+Mn+Mg+Ca)$]. Arrows show chemical zoning from core (c) to rim (r) of representative garnet porphyroblasts

Omphacite

Figure 4 shows clinopyroxene compositions from each sample; the Fe^{2+}/Fe^{3+} ratio and end-member components were calculated following *Harlow* (1999).

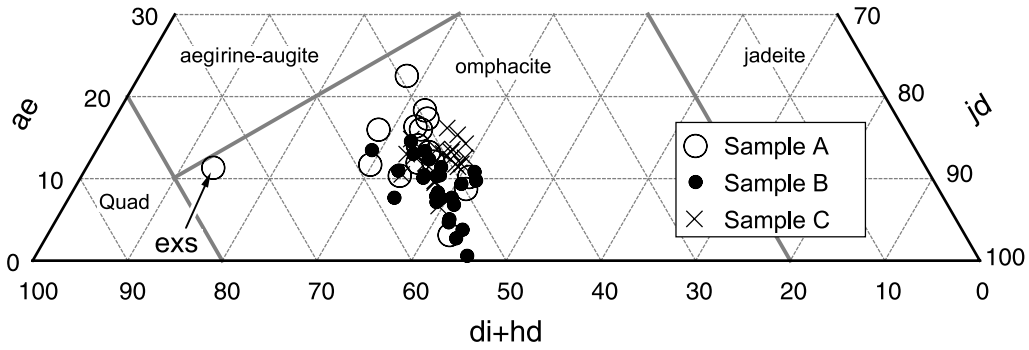

Fig. 4. Compositional trends of clinopyroxene in investigated rocks from Tiburon. *jd* jadeite, *ae* aegirine, *di + hd* diopside and hedenbergite, *exs* exsolution, *Quad* Ca–Mg–Fe pyroxenes

Omphacite in sample A is $jd_{27-40}di + hd_{47-59}ae_{3-22}$; the X_{Mg} ranges from 0.73 to 0.88, and contains rare irregular-shaped patches (<20 μm) of jadeite-poor omphacite ($jd_{13}di + hd_{75}ae_{12}$). Omphacite in sample B is $jd_{28-43}di + hd_{73}ae_{1-15}$, with $X_{Mg} = 0.77–0.92$. Omphacite in sample C has similar compositions to that of samples A and B ($jd_{33-39}di + hd_{47-55}ae_{7-16}$; $X_{Mg} = 0.75–0.87$). Ca-Tschermak component of omphacite in all lithologies is less than 2 mol%.

Amphiboles

Compositions of sodic amphiboles are plotted in Fig. 5; the structural formulae of amphiboles were calculated based on O = 23 and the Fe^{2+}/Fe^{3+} ratio was estimated based on total cation = 13 excluding Ca, Na and K. Hornblende in sample A is magnesio-katophorite to taramite, with Si = 6.5–6.7 p.f.u., $^{[B]}$Na (Na in the B-site) = 0.60–0.67, and $^{[A]}(Na + K) = 0.61–0.81$; X_{Mg} ranges from 0.60 to 0.69. Al_2O_3 and TiO_2 contents reach 11.1 and 0.8 wt%, respectively; the Ti content slightly decreases toward the rim. Glaucophane in sample A is characterized by 0.10–0.43 p.f.u. Ca and 0.6–0.29 p.f.u. $^{[4]}$Al, with $X_{Mg} = 0.56–0.70$. The inferred $Fe^{3+}/(Fe^{3+} + {}^{[6]}Al)$ ratio ranges from 0.17 to 0.24. Inclusion glaucophane within omphacite contains up to 2.8 wt.% CaO. Hornblende in sample B is barroisite, with Si = 6.7 p.f.u., $^{[B]}$Na (Na in the B-site) = 0.92–0.94, and $^{[A]}(Na + K) =$ 0.40–0.48; X_{Mg} is 0.60–0.61. Glaucophane within garnet in sample B is characterized by 0.03 p.f.u. Ca and 0.01 p.f.u. $^{[4]}$Al, with $X_{Mg} = 0.58$ and $Fe^{3+}/(Fe^{3+} + {}^{[6]}Al) = 0.08$. Glaucophane in sample C is characterized by 0.04–0.25 p.f.u. Ca and 0–0.18 p.f.u. $^{[4]}$Al, with $X_{Mg} = 0.54–0.67$ and $Fe^{3+}/(Fe^{3+} + {}^{[6]}Al) = 0.02–0.21$. Inclusion glaucophane within omphacite has slightly higher X_{Mg} value.

Phengite

Phengite in samples A and B contains 3.39–3.47 Si p.f.u. (O = 11) and low Na/(Na + K) (0.01–0.03); X_{Mg} varies from 0.66 to 0.73 (Fig. 6). In sample C, inclusion phengite contains up to 3.49 Si p.f.u., whereas retrograde phengite in the matrix is Si-poor (3.29–3.34 p.f.u.).

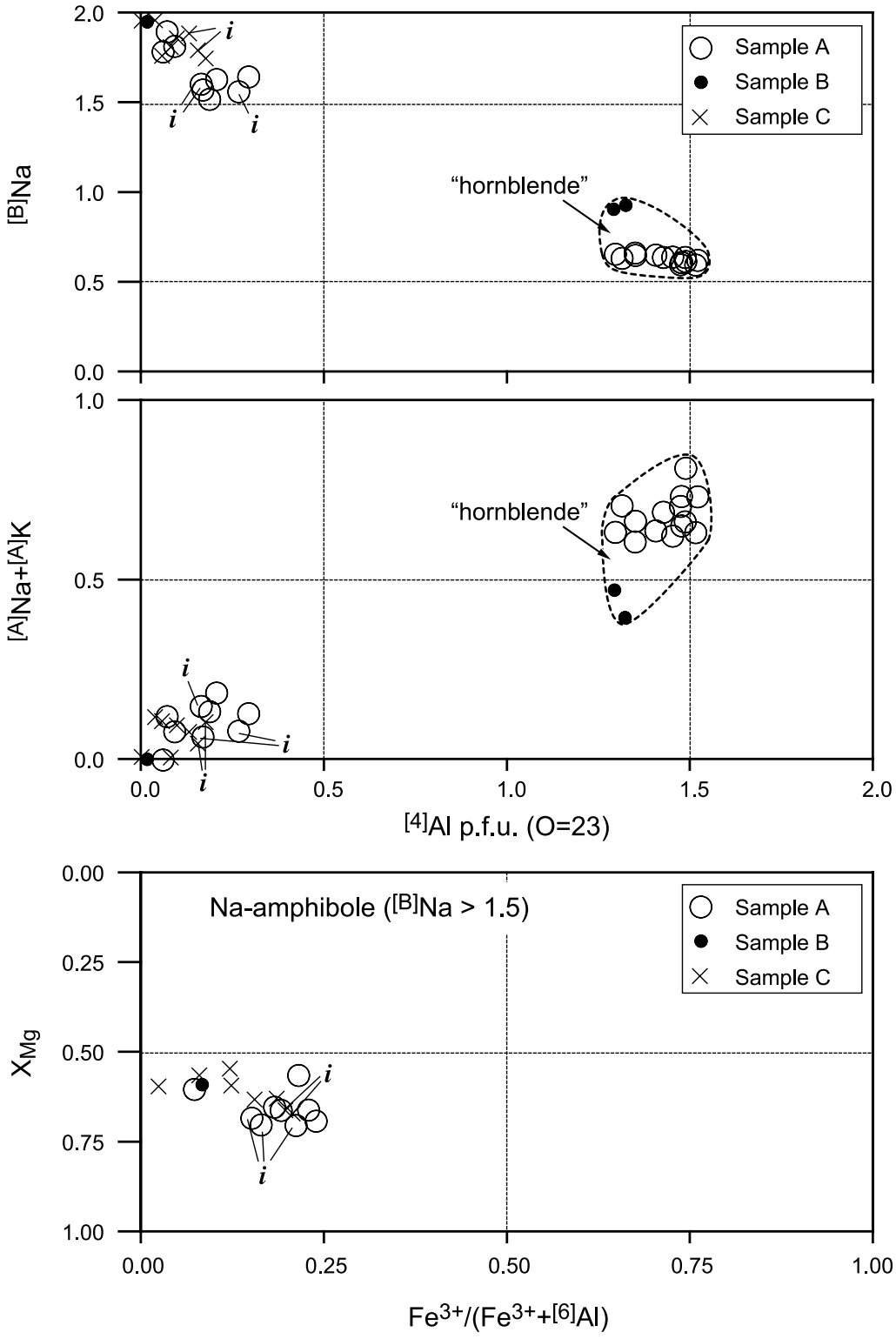

Fig. 5. Compositional variations of amphiboles in investigated rocks from Tiburon. *i* Inclusion within omphacite

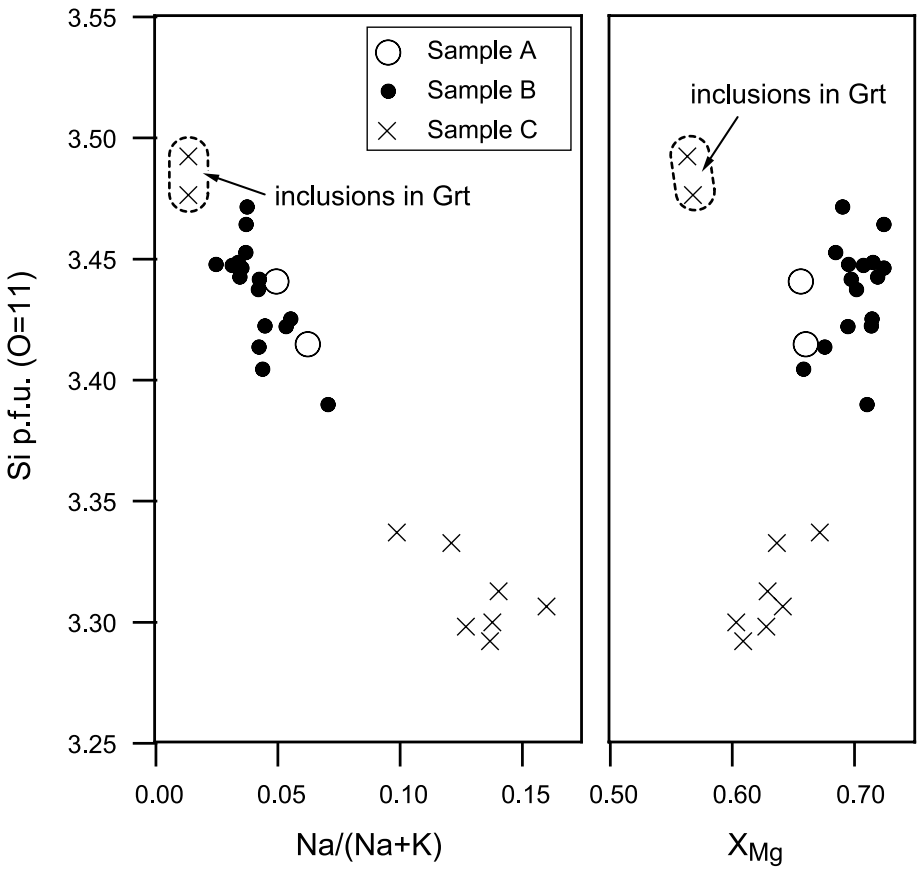

Fig. 6. Compositional variations of phengite in investigated rocks from Tiburon. *i* Inclusion within garnet

Epidote

Epidote in samples A and C shows similar compositional range; the $Y_{Fe^{3+}}$ [$= Fe^{3+}/(Fe^{3+} + Al)$] varies from 0.16 to 0.18. Epidote in sample B is characterized by a wider range of $Y_{Fe^{3+}}$ (0.14–0.20). No apparent difference in composition exists among different textural types of epidote in individual samples.

Other minerals

Paragonite inclusions within omphacite-I in sample B are characterized by low $K/(K + Na)$ (0.05). Chlorite is characterized by moderate Si (5.6–5.7 p.f.u. for $O = 28$) and Al (4.7–4.9 p.f.u.); X_{Mg} varies from 0.45 to 0.62. Titanite in all samples contains 0.9–1.4 wt.% Al_2O_3.

New K–Ar dating

We newly obtained K–Ar hornblende and phengite ages from our sample A [= "TIBB" (*Wakabayashi*, 1990) = "PG23" (*Anczewicz* et al., 2004)]. The K–Ar dating was carried out at Okayama University of Science following analyt-

Table 2. *K–Ar ages of epidote-amphibolitic eclogite (sample A) from Tiburon*

Mineral	K (wt.%)	Rad.^{40}Ar (10^{-8} cc STP/g)	Non rad. Ar (%)	Age (Ma)
Hornblende	0.435 ± 0.02	289.7 ± 2.9	9.3	152.8 ± 7.5
Phengite	8.66 ± 0.17	5501 ± 53	2.3	153.1 ± 3.3

ical procedures by *Tsujimori* and *Itaya* (1999). The results are 153 ± 7.5 Ma for hornblende ($K = 0.43 \pm 0.02$ wt.%) and 153 ± 3.3 Ma for phengite ($K = 8.7 \pm 0.17$ wt.%) (Table 2). These data overlap with Lu–Hf garnet ages of the same block (153.4 ± 0.8 Ma) and an eclogite block from Jenner (157.9 ± 0.7 Ma) (*Anczie wicz* et al., 2004).

P–T conditions of metamorphism

Thermobarometry for eclogite-facies metamorphism

In the investigated samples, the eclogite-facies stage is characterized by the Grt + Omp + Ep + Gln ± Hbl ± Pg + Phe + Qtz + Rt assemblage; this assemblage is common in low-*T* eclogites of HP terranes throughout the world (e.g., *Clarke* et al., 1997; *Matsumoto* et al., 2003; *Tsujimori*, 2002; *Tsujimori* and *Liou*, 2005; *Rad* et al., 2005). *P–T* conditions for the peak eclogite-facies stage are constrained by Fe–Mg exchange mineral thermobarometers and mineral equilibria. In spite of different samples, the Fe^{2+}–Mg distribution coefficient (K_D) between garnet rim and adjacent omphacite varies from 10 to 21 [$\ln(K_D) = 2.5$ to 3.0], and yields temperature at $P = 2$ GPa of 510–630 °C, applying the calibration of *Krogh Ravna* (2000); the Grt-Cpx thermometry by *Ellis* and *Green* (1979) yields about 50 °C higher temperature, consistent with a previous estimate by *Wakabayashi* (1990). Temperature variation might be caused mainly by uncertainty in estimation of the Fe^{2+}/Fe^{3+} ratio of omphacite. The Grt-Cpx-Phe thermobarometry (*Krogh Ravna* and *Terry*, 2004) yields

Table 3. *Summary of estimated eclogite-facies P–T conditions of the investigated samples*

	Grt-Cpx-Phe (i)	Grt-Cpx-Phe (ii)	TC average *P–T*
Sample A			
peak EC stage	2.3–2.6 GPa (at 550–620 °C)	2.2 GPa (at 550–620 °C)	2.5 ± 0.2 GPa, 570 ± 30 °C
Sample B			
peak EC stage	2.4–2.5 GPa (at 550–620 °C)	2.1 GPa (at 550–620 °C)	2.6 ± 0.2 GPa, 620 ± 30 °C
pre-peak EC stage			1.8 ± 0.2 GPa, 490 ± 70 °C
Sample C			
peak EC stage	2.3–2.4 GPa (at 550–620 °C)	1.9–2.0 GPa (at 550–620 °C)	2.3 ± 0.2 GPa, 570 ± 30 °C

(i) *Krogh Ravna* and *Terry* (2004); (ii) *Waters* and *Martin* (1993). *TC* THERMOCALC

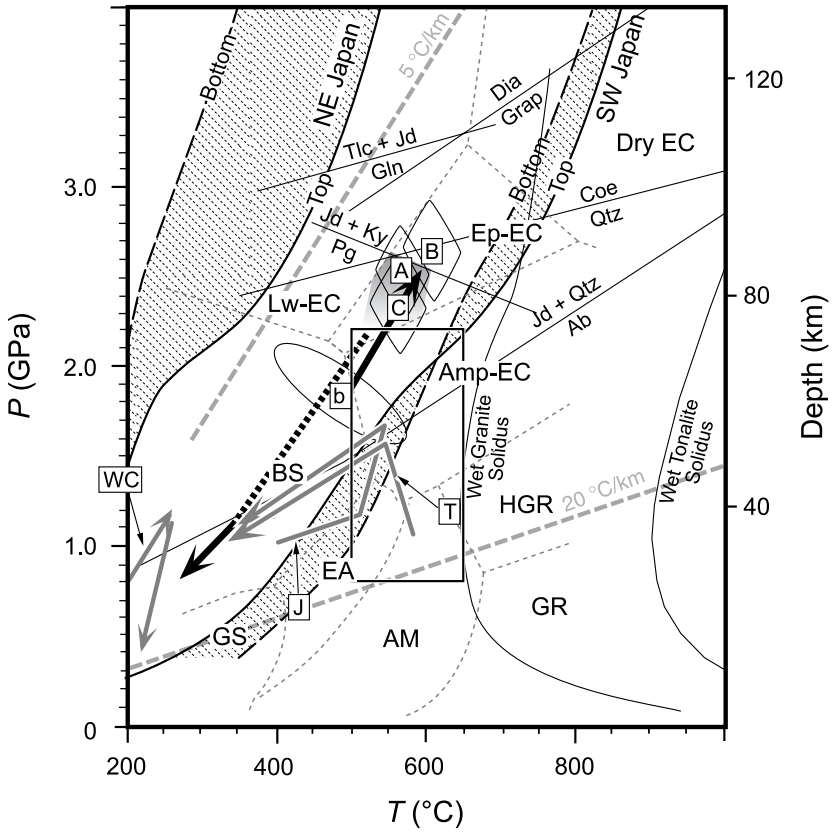

Fig. 7. *P–T* diagram showing eclogite-facies *P–T* condition (gray-gradiented area) and qualitative *P–T* path of the Tiburon eclogite (heavy arrows); *A* sample A, *B* sample B, *C* sample C. The uncertainty in *P–T* estimates calculated by THERMOCALC is indicated by the size of the ellipse (1σ). The 'b' represents the *P–T* condition of inclusion garnet and host omphacite omphacite-I with old schistosity of sample B. The inferred *P–T* paths of exotic high-grade eclogite blocks (J: *Krogh* et al., 1994; T: *Wakabayashi*, 1999) and coherent low-grade blueschist (WC: *Banno* et al., 2000) from the Franciscan Complex are also shown (gray arrows). Hatched areas represent the calculated *P–T* conditions for oceanic crust beneath present-day NE Japan ('cold') and SW Japan ('warm') subduction zones (*Peacock* and *Wang*, 1999); the solid and dashed lines show the top and bottom of oceanic crust. The metamorphic facies and their abbreviations are after *Liou* et al. (2004). The box represents a *P–T* space of *P–T* pseudosections shown in Fig. 8

$P = 2.4$–2.6 GPa and $T = 550$–620 °C (Table 3; Fig. 7), while the calibration proposed by *Waters* and *Martin* (1993) suggests $P = 1.9$–2.2 GPa at the same temperature range. In general, the celadonite component of phengite is the most sensitive to pressures (e.g., *Massonne* and *Schreyer*, 1987; *Carswell* et al., 1997; *Krogh Ravna* and *Terry*, 2004). In some Franciscan retrograded eclogites, Si-rich phengites, in disequilibrium with the eclogitic mineral assemblage, formed during blueschist-facies overprinting (e.g., *Moore*, 1984; *Tsujimori* et al., in press). The investigated Tiburon eclogites also experienced blueschist-facies overprinting. However, the retrograde phengite in Tiburon eclogites is characterized by a lower Si content, as we found a distinct compositional difference

between inclusion phengite within the garnet rim and matrix retrograde phengite in sample C (Fig. 6). Therefore, it is unlikely that the Si-rich phengite that we used to obtain pressure was at disequilibrium with the eclogitic mineral assemblage.

In addition to the Grt-Cpx-Phe thermobarometry, the program THERMOCALC (ver. 2.75) (*Holland* and *Powell*, 1998; *Powell* et al., 1998) and the internally consistent thermodynamic dataset (20 April 1996) were used to estimate *P–T* conditions. The THERMOCALC average-*P–T* calculation mode was applied for the assemblage Grt + Omp + Hbl (or Gln) + Ep + Phe; activities of mineral end-members were obtained using the program AX recommended by *Holland* and *Powell* (1998). The fluid composition was assumed to be pure H_2O. The results of average-*P–T* calculations of each sample are comparable with the Grt-Cpx-Phe thermobarometry by *Krogh Ravna* and *Terry* (2004) (Table 3; Fig. 7). Although the sample B yields a pressure of up to 2.6 GPa, its uncertainty overlaps the paragonite stability field. The preferred peak stage conditions are about $P = 2.2$–2.5 GPa, $T = 550$–$620\,^{\circ}C$; the presence of paragonite in sample B implies that the maximum peak pressure is limited by the reaction $Pg = Jd + Ky + H_2O$ (*Holland*, 1979; *Tropper* and *Manning*, 2004). In sample B, coarse-grained omphacite porphyroblasts contain inclusions of garnet and paragonite, which represent a prograde stage (together with epidote + quartz), for which pre-peak conditions of $P = 1.8 \pm 0.2$ GPa and $T = 490 \pm 70\,^{\circ}C$ were calculated with THERMOCALC average-*P–T* (Table 3; Fig. 7).

P–T conditions of blueschist-facies overprinting

Blueschist-facies overprinting is a common feature in many Franciscan high-grade blocks (cf., *Wakabayashi*, 1999). Such a *P–T* path suggests that the rocks have been ''refrigerated'' during exhumation (*Ernst*, 1988); hence no greenschist- or albite-epidote-amphibolite facies recrystallization took place. The blueschist-facies stage is characterized by M_2 minerals that include chlorite, titanite, glaucophane, epidote, phengite and rare titanite. The breakdown of rutile is critical to defining this later blueschist-facies recrystallization. The mineral assemblage suggests M_2 minerals crystallized within the Chl + Gln ± Ab stability field of the epidote-blueschist facies (e.g., *Evans*, 1990; *Frey* et al., 1991) ($P = 0.7$–1.1 GPa and $T = \sim 350\,^{\circ}C$) (Fig. 7). The experimentally determined reaction by *Maruyama* et al. (1986).

$$9\ \text{clinochlore} + 6\ \text{tremolite} + 50\ \text{albite} = 25\ \text{glaucophane} + 6\ \text{clinozoisite} + 7\ \text{quartz} + 14\ H_2O$$

constrains the minimum $P > 0.7$–0.8 GPa at $T = \sim 350\,^{\circ}C$ for the retrograde mineral assemblages of samples A and C. Irregular patches of jadeite-poor omphacite in sample A may have exsolved from eclogitic omphacite during this stage; the exsolution feature of omphacite implies low-*T* blueschist-facies condition of $T < 350\,^{\circ}C$ (e.g., *Tsujimori* and *Liou*, 2004; *Tsujimori* et al., 2005, in press). Although the investigated eclogites do not contain retrograde lawsonite in the blueschist-facies stage, lawsonite veins and lawsonite replacing eclogitic garnet are common in some Tiburon eclogites (e.g., *Wakabayashi*, 1990) as Ring Mountain is

the type locality for lawsonite (*Ransome*, 1894). Blueschist-facies overprinting may have occurred in the lawsonite-stability field and subsequent fluid infiltration may have formed lawsonite veins at $T < 300\,^{\circ}C$ (*Liou*, 1971). The lack of retrograde lawsonite in the investigated samples could be due to H_2O undersaturation during recrystallization.

Phase relations of Tiburon eclogites in the system Na_2O–CaO–FeO–MgO–Al_2O_3–SiO_2–H_2O

In Ring Mountain, the hornblende-rich sample A (''TIBB'' of *Wakabayashi*, 1990) exhibits different petrographic features from samples B and C, in that epidote-amphibolitic minerals are the dominant mineral assemblage. However, our *P*–*T* estimate for the peak eclogite-facies stage is similar to the other samples. Can the difference be explained by different bulk rock composition rather than different physical condition? To answer this question, *P*–*T* pseudosections were calculated using the program THERMOCALC; two bulk rock compositions of Tiburon eclogite from *Saha* et al. (2005) were used for the calculation (Fig. 8). In the Franciscan eclogite (*sensu lato*), the major constituent minerals are garnet, omphacite, epidote, lawsonite, hornblende (Ca–Na amphibole), glaucophane, paragonite, phengite, chlorite, rutile, titanite, albite and quartz (e.g., *Oh* and *Liou*, 1990; *Wakabayashi*, 1990; *Krogh* et al., 1994; *Shibakusa* and *Maekawa*, 1997). For the calculation, we assumed the model system Na_2O–CaO–FeO–MgO–Al_2O_3–SiO_2–H_2O (NCFMASH) and selected the following phases: omphacite, garnet, hornblende, glaucophane, paragonite, zoisite (representing epidote in Fe^{3+}-free model system), lawsonite, kyanite, albite, quartz and water. We also considered excess quartz and water (pure H_2O). Mineral activity-composition models followed *Carson* et al. (1999). Fe_2O_3 is neglected because of a lack of sufficient thermodynamic data for Fe^{3+}-bearing mineral end-members. This will significantly affect the stability of Fe^{3+}-bearing minerals (*LeVay* and *Kerrick*, 2005), particularly in the epidote stability field (e.g., *Evans*, 1990; *Tsujimori* and *Ishiwatari*, 2002; *Tsujimori* and *Liou*, 2004b; *Mattinson* et al., 2004). In natural parageneses, moreover, H_2O undersaturation and fO_2 can strongly affect the epidote stability field (e.g., *Poli* and *Schmidt*, 1997; *Liou* et al., 2004). However, in general, the topology of calculated phase relationships in *P*–*T* space is applicable to discuss the observed petrographic characteristics (e.g., *Carson* et al., 1999, 2000; *Wei* et al., 2003).

A calculated *P*–*T* projection in the range $P = 0.8$–2.2 GPa and $T = 500$–$650\,^{\circ}C$ showing the NCFMASH univariant reactions and invariant points is given in Fig. 8a. Similar phase relations have been calculated by *Carson* et al. (1999) and *Hoschek* (2001), although their petrogenetic grids include chlorite as an additional phase. Furthermore, all univariant reactions have been inferred to be stable in the NCFMASH system (e.g., *Will* et al., 1998; *Carson* et al., 1999). Our observations together with the previous observation by *Wakabayashi* (1990) indicate that Tiburon eclogites did not cross over the univariant lines to enter the kyanite or lawsonite stability fields (Figs. 7 and 8a).

The bulk rock composition used in Fig. 8b is Al_2O_3 19.70 mol%, CaO 24.56 mol%, MgO 29.23 mol%, FeO 21.06 mol% and Na_2O 5.45 mol% (''TIBB''

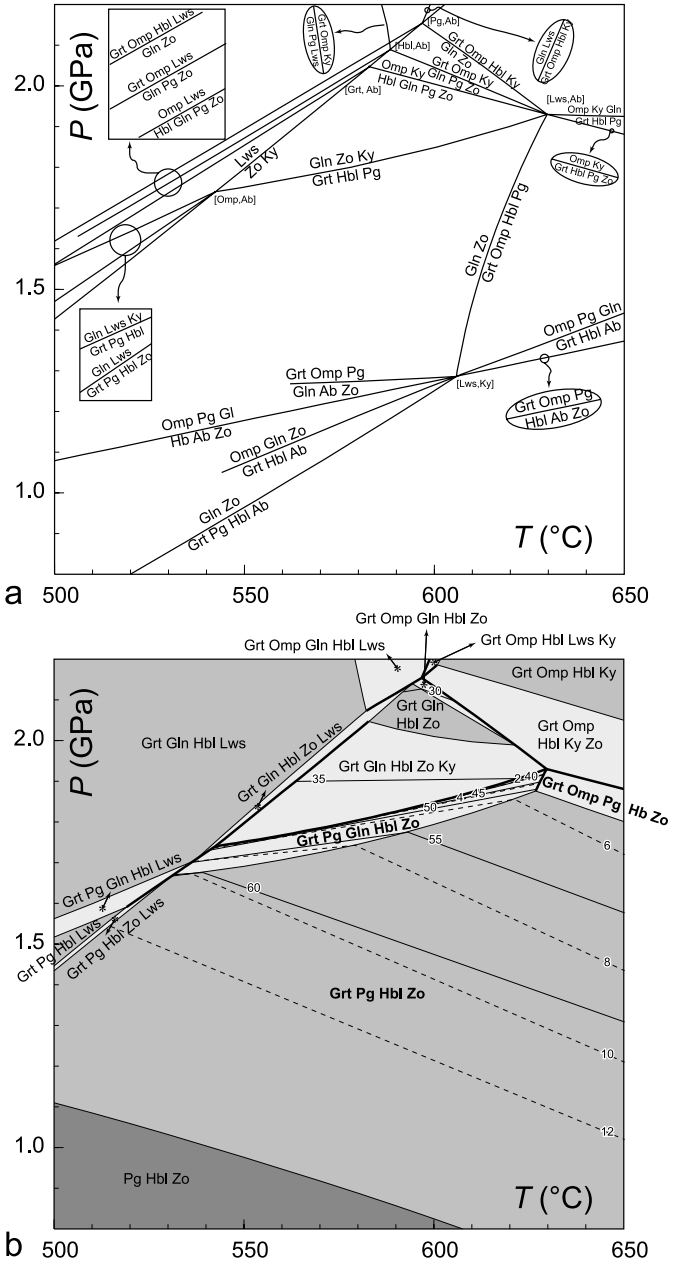

Fig. 8. *P–T* projection and pseudosections in NCFMASH (+Qtz + H_2O). Note that the calculated *P–T* pseudosections do not fit with either generic petrogenetic grid or our *P–T* estimation but the topology of calculated phase relationships in *P–T* space is applicable for discussion. (**a**) *P–T* projection for the full system NCFMASH is projected from quartz and H_2O. (**b**) *P–T* pseudosection for a bulk rock composition of garnet amphibolite block of ''TIBB'' in *Saha* et al. (2005), Al_2O_3:CaO:MgO:FeO:Na_2O = 19.70:24.56:29.23:21.06:5.45; this block is from the same block as sample A. Modal amounts of paragonite (thin dashed lines) and hornblende (thin lines) are contoured. (**c**) *P–T* pseudosection for a bulk rock composition of less retrograded eclogite (''EC'' in *Saha* et al., 2005), Al_2O_3:CaO:MgO:FeO:Na_2O = 23.49:33.38:22.44:12.63:8.07; this bulk-rock composition may be appropriate for sample B

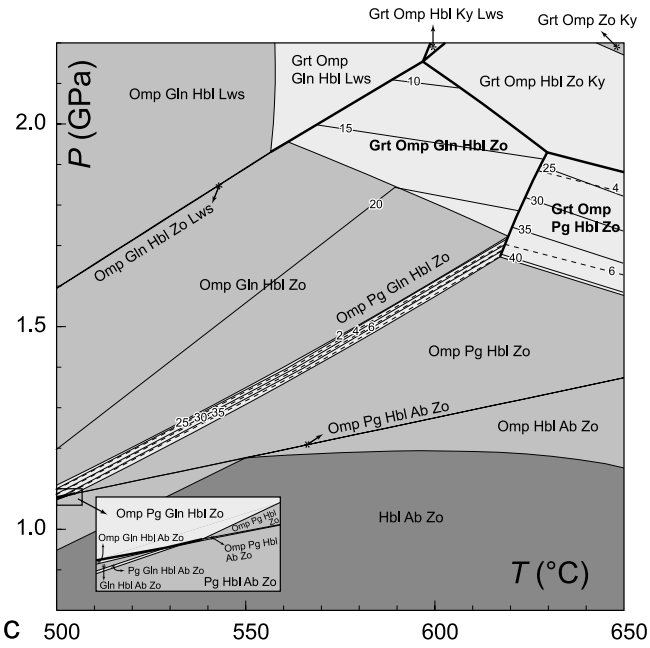

Fig. 8 (*continued*)

sample of *Saha* et al., 2005); this bulk rock composition represents the TIBB block of *Wakabayashi* (1990) and our sample A. In the *P–T* pseudosection for a garnet-amphibolite of ''TIBB'' in *Saha* et al. (2005) (Fig. 8b), a wide trivariant *P–T* field of Grt + Pg + Hbl + Zo is comparable to the $M_0{}^A$ assemblage Hbl + Ep + Grt-I + Rt + Qtz of our sample A; it may also explain abundant epidote amphibolitic assemblage ($M_0{}^A$). Although paragonite was not yet found in the $M_0{}^A$ assemblage, this phase may have been consumed to form the $M_1{}^A$ assemblage of eclogite-facies and/or has been replaced during latest blueschist-overprinting stage ($M_2{}^A$). Moreover, the calculated modal amount of paragonite in the *P–T* pseudosection of Fig. 8b suggests only minor paragonite is predicted to occur in the eclogitic *P–T* condition. The bulk rock composition used in Fig. 8c is Al_2O_3 23.49 mol%, CaO 33.38 mol%, MgO 22.44 mol%, FeO 12.63 mol% and Na_2O 8.07 mol% (''EC'' sample of *Saha* et al., 2005); this composition represents less retrograded Tiburon eclogites and is similar to our sample B. By comparing the *P–T* pseudosection for the ''TIBB'' bulk composition, this shows a wide *P–T* stability range for omphacite (Fig. 8c). In particular, divariant fields of Grt + Omp + Gln + Hbl + Zo and Grt + Omp + Pg + Hbl + Zo are consistent with our sample B as well as eclogitic-stage mineral assemblage in most Franciscan eclogites (e.g., *Oh* and *Liou*, 1990; *Wakabayashi*, 1990; *Krogh* et al., 1994); if bulk FeO becomes higher, a trivariant field of Grt + Omp + Gln + Zo appears in the high-pressure divariant field of Grt + Omp + Gln + Hbl + Zo (*Tsujimori* and *Matsumoto*, 2006).

Although natural parageneses might be affected by heterogeneity of the effective bulk-rock compositions, geothermobarometry and tentative *P–T* pseudosection analyses suggest that the different eclogitic blocks of Tiburon likely experienced similar eclogite-facies and subsequent retrograde metamorphism.

Discussions

New insights

Our new petrologic examinations of three samples together with previous work by *Wakabayashi* (1990) in Ring Mountain constrain the *P–T* history during the subduction and exhumation of Tiburon eclogite. As described above, the epidote amphibolitic mineral assemblage in sample A has been considered as precursor that formed in a higher geotherm (e.g., *Oh* and *Liou*, 1990; *Wakabayashi*, 1990; *Krogh* et al., 1994). However, our *P–T* pseudosection analyses (Fig. 8) suggest that the epidote amphibolitic assemblage was stable at eclogite-facies conditions. In fact, katophoritic or barroisitic amphiboles occur in low-temperature eclogite (e.g., *Clarke* et al., 1997; *Wei* et al., 2003). The earlier schistosity $S_0{}^A$ with $M_0{}^A$ assemblage in sample A may be comparable to internal fabric $S_0{}^B$ within porphyroclastic omphacite-I of sample B. The inferred *P–T* path of Tiburon eclogite characterized by a counterclockwise hairpin *P–T* trajectory is shown in Fig. 7. In our interpretation, prograde eclogite-facies metamorphism produced both eclogitic and epidote amphibolitic assemblages in a similar loading *P–T* path (Fig. 7). This is supported by the presence of prograde-zoned garnets and the absence of prograde albite in epidote amphibolitic assemblages (e.g., *Wakabayashi*, 1990; *Krogh* et al., 1994). Furthermore, our K–Ar hornblende age from epidote amphibolitic assemblages is identical to the Lu–Hf ages of eclogite-facies metamorphism of Franciscan high-grade blocks (*Anczewicz* et al., 2004).

What is the pressure maximum of Franciscan eclogite? How deep have Franciscan eclogites been subducted? Our reevaluation of eclogite-facies metamorphism recorded in Tiburon eclogite suggests peak conditions at $P = 2.2–2.5$ GPa and $T = 550–620$ °C; this *P–T* estimate indicates that Tiburon high-grade blocks were subducted to depths of approximately 75 km. Considering similarities of mineral parageneses and compositions, most Franciscan eclogites may record similar eclogite-facies metamorphism at such mantle depths. The inferred loading *P–T* trajectory lies between the calculated ''warm'' and ''cold'' subduction zone geotherm by *Peacock* and *Wang* (1999) (Fig. 7). On the other hand, the high-*T* garnet-clinopyroxene amphibolite assemblage in some Franciscan high-grade blocks (e.g., *Hermes*, 1973; *Wakabayashi*, 1987 and unpubl. data; *Anczewicz* et al., 2004; *Tsujimori* et al., in press) is characterized by Ti-rich brown pargasite, augite, garnet, and plagioclase (pseudomorph), and represents nearly HP granulite-facies metamorphism formed at $T = \sim 600–700$ °C and $P = 0.7–1.0$ GPa (e.g., *Pattison*, 2003; *Zhang* et al., 2006). Plagioclase-bearing garnet amphibolites are interpreted as a variety of high-*T* amphibolite and experienced a different tectonometamorphic history except for blueschist-facies overprinting. Tiburon eclogites record lower geothermal gradients relative to these high-*T* amphibolites that have blueschist overprints but lack eclogitic assemblages (*Wakabayashi*, 1990). This is likely to support a model of a decreasing geotherm during continuous subduction (e.g., *Wakabayashi*, 1990; *Anczewicz* et al., 2004).

Tectonic implications

Recently, *Anczewicz* et al. (2004) reported Lu–Hf ages for eclogite (158–153 Ma), high-*T* amphibolite (169–163 Ma), and blueschist (147 Ma) from the Franciscan

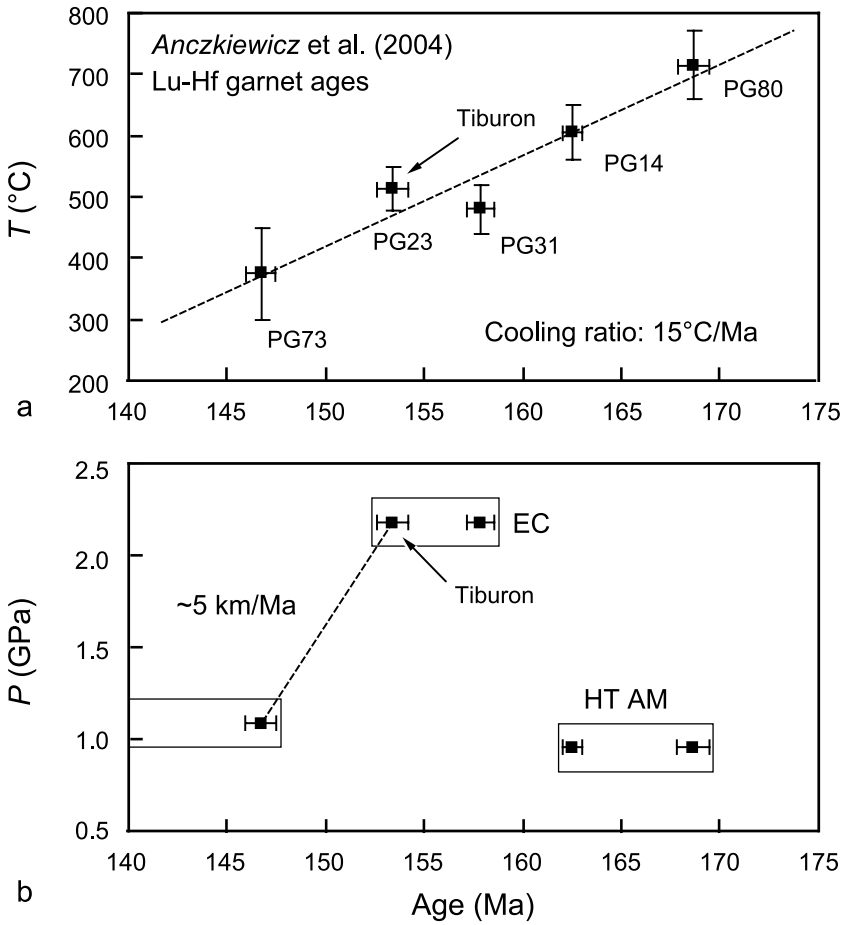

Fig. 9. (**a**) Age versus peak temperature diagram showing possible cooling rate (ca. 15 °C/km) of early Franciscan subduction by *Anczkiewicz* et al. (2004). (**b**) Age versus peak pressure diagram showing possible exhumation rate of Tiburon eclogite

complex at several localities. They pointed out an interesting correlation between age and temperature (Fig. 9a), and suggested a cooling rate along the subduction zone interface from amphibolite to blueschist facies conditions of about 15 °C/Ma. Taking the age data of *Anczewicz* et al. (2004) with our qualitative pressure estimates into account, we obtained a relationship between age and pressure as shown in Fig. 9b. Their sample ''PG23'' is the same block that was collected and labeled ''sample A'' in this study. In Fig. 9b, if we assume that 153.4 Ma as the timing for peak metamorphism *P* at 2.2–2.5 GPa and the timing of the blueschist-facies overprinting with the same age of the coherent blueschist at 146.7 Ma, about 34 km of exhumation must have occurred within about 6 Ma. This leads to an average exhumation rate of ~5 km/Ma, similar to those calculated for the Kokchetav and Sulu UHP terranes (*Katayama* et al., 2001; *Liu* et al., 2003). Such a high exhumation rate is consistent with the observations of exposure and erosion of some high-grade blocks as early as Tithonian-Valanginian time (see discussion in *Wakabayashi* and *Dilek*, 2003). At least part of such fast exhumation may have been related to forearc serpentinite mud volcanism as envisaged by *Fryer* et al. (2000). Our new

K–Ar ages and the Lu–Hf garnet age of *Anczie wicz* et al. (2004) also support a rapid exhumation rate. It should be noted, however, that the blueschist-facies overprinting of high-grade blocks may have occurred at least as old as 159 Ma and as young as 138 Ma (*Wakabayashi*, 1999), so the matching of a ca. 147 Ma blueschist age from a coherent thrust sheet in the Panoche Pass area with a ca. 153 Ma eclogite age from Tiburon Peninsula may not be valid. It is likely that a variety of retrograde *P–T-t* paths characterize numerous Franciscan high-grade blocks.

Acknowledgements

This research was supported by the Japanese Society for the Promotion of Science through Research Fellowship for Research Abroad for the first author (Tsujimori) and Grant-in-Aid of Fukada Geological Institute for the second author (Matsumoto). The authors also acknowledge support by the National Science Foundation through NSF grant EAR-0510325 (Liou). We thank T. Itaya for providing facility for the K–Ar dating and R. G. Coleman, C. W. Oh, A. Proyer for detailed review of the manuscript.

References

Anczkiewicz B, Platt JP, Thirlwall MF, Wakabayashi J (2004) Franciscan subduction off to a slow start: evidence from high-precision Lu–Hf garnet ages on high grade-blocks. Earth Planet Sci Lett 225: 147–161

Armstrong JT (1988) Quantitative analysis of silicate and oxide minerals: comparison of Monte Carlo, ZAF and Phi-Rho-Z procedure. In: *Newbury DE* (ed) Analysis Microbeam, San Francisco Press, California, pp 239–246

Banno S, Shibakusa H, Enami M, Wang CL, Ernst WG (2000) Chemical fine structure of Franciscan jadeitic pyroxene from Ward Creek, Cazadero area, California. Am Mineral 85: 1795–1798

Blake MC Jr., Jayko AS, McLaughlin RJ, Underwood MB (1988) Metamorphic and tectonic evolution of the Franciscan Complex, northern California. In: *Ernst WG* (ed) Metamorphism and crustal evolution of the western United States, Rubey Volume VII, pp 1035–1060

Carson CJ, Powell R, Clarke GL (1999) Calculated mineral equilibria for eclogites in $CaO–Na_2O–FeO–MgO–Al_2O_3–SiO_2–H_2O$: application to the Pouébo Terrane, Pam Peninsula, New Caledonia. J Metamorph Geol 17: 9–24

Carson CJ, Clarke GL, Powell R (2000) Hydration of eclogite, Pam Peninsula, New Caledonia. J Metamorph Geol 18: 79–90

Carswell DA, Obrien PJ, Wilson RN, Zhai M (1997) Thermobarometry of phengite-bearing eclogites in the Dabie Mountains of central China. J Metamorph Geol 15: 239–252

Catlos EJ, Sorensen SS (2003) Phengite-based chronology of K- and Ba-rich fluid flow in two paleosubduction zones. Science 299: 92–95

Clarke GL, Aitchison JC, Cluzel D (1997) Eclogites and blueschists of the Pam Peninsula, NE New Caledonia: a reappraisal. J Petrol 38: 843–876

Coleman RG, Lanphere MA (1971) Distribution and age of high-grade blueschists associated eclogites, and amphibolites from Oregon and California. Geol Soc Am Bull 82: 2397–2412

Coleman RG, Lee DE, Beatty LB, Brannock WW (1965) Eclogites and eclogites: their differences and similarities. Geol Soc Am Bull 76: 486–508

Ellis DJ, Green DH (1979) An experimental study of the effect of Ca upon garnet-clinopyroxene Fe–Mg exchange equilibria. Contrib Mineral Petrol 71: 13–22

Ernst WG (1988) Tectonic history of subduction zones inferred from retrograde blueschist P–T paths. Geology 16: 1081–1084

Evans BW (1990) Phase relations of epidote-blueschists. Lithos 25: 3–23

Frey M, de Capitani C, Liou JG (1991) A new petrogenetic grid for low-grade metabasites. J Metamorph Geol 9: 497–509

Fryer P, Lockwood JP, Becker N, Phipps S, Todd CS (2000) Significance of serpentine mud volcanism in convergent margins: In: *Dilek Y, Moores EM, Elthon D, Nicolas A* (eds) Ophiolites and Oceanic Crust: New Insights from Field Studies and the Ocean Drilling Program, Geol Soc Am Spec Paper 349, pp 35–51

Hanan BB, Kimbrough DL, Renne PR (1992) The Stonyford Volcanic Complex: a Jurassic seamount in the Northern California Coast Ranges. Am Assoc Petroleum Geol Bull 76: 421–432

Harlow GE (1999) Interpretation of Kcpx and CaEs components in clinopyroxene from diamond inclusions and mantle samples. In: *Gurney JJ, Gurney JL, Pascoe MD, Richardson SH* (eds) Proceedings of Seventh International Kimberlite Convention, Vol. I. Redroof Design Cc, Cape Town, pp 321–331

Hermes OD (1973) Paragenetic relationships in an amphibolitic tectonic block in the Franciscan terrain, Panoche Pass, California. J Petrol 14: 1–32

Holland TJB (1979) The experimental determination of the reaction paragonite = jadeite + kyanite + H_2O and internally consistent thermodynamic data for part of the system Na_2O–Al_2O_3–SiO_2–H_2O, with applications to eclogites and blueschists. Contrib Mineral Petrol 68: 293–301

Holland TJB, Powell R (1998) An internally consistent thermodynamic data set for phases of petrological interest. J Metamorph Geol 19: 309–343

Hopson CA, Pessagno EA Jr, Mattinson JM, Luyendyk BP, Beebe W, Hull DM, Munoz IM, Blome CD (1996) Coast Range ophiolite as paleoequatorial mid-ocean lithosphere. GSA Today 6: 3–4

Hoschek G (2001) Thermobarometry of metasediments and metabasites from the Eclogite zone of the Hohe Tauern, Eastern Alps, Austria. Lithos 59: 127–150

Hoschek G (2004) Comparison of calculated P–T pseudosections for a kyanite eclogite from the Tauern Window, Eastern Alps, Austria. Eur J Mineral 16: 59–72

Kretz R (1983) Symbols for rock-forming minerals. Am Mineral 68: 277–279

Krogh EJ, Oh CW, Liou JG (1994) Polyphase and anticlockwise P–T evolution for Franciscan eclogites and blueschists from Jenner, California, USA. J Metamorph Geol 12: 121–134

Krogh Ravna E (2000) The garnet-clinopyroxene Fe^{2+}–Mg geothermometer: an updated calibration. J Metamorph Geol 18: 211–219

Krogh Ravna E, Terry MP (2004) Geothermobarometry of UHP and HP eclogites and schists – an evaluation of equilibria among garnet-clinopyroxene-kyanite-phengite-coesite/quartz. J Metamorph Geol 22: 579–592

Leake BE, Woolley AR, Arps CES, Birch WD, Gilbert MC, Grice JD, Hawthorne FC, Kato A, Kisch HJ, Krivovichev VG, Linthout K, Laird J, Mandarino JA, Maresch WV, Nickel EH, Rock NMS, Schumacher JC, Smith DC, Stephenson NCN, Ungaretti L, Whittaker EJW, Guo YZ (1997) Nomenclature of amphiboles: Report of the subcommittee on amphiboles of the International Mineralogical Association, commission on new minerals and mineral names. Am Mineral 82: 9–10

LeVay B, Kerrick DM (2005) Thermodynamic computation of eclogite phase equilibria: The key role of redox state. Mitt Österr Miner Ges 150: 86

Liou JG (1971) P–T Stabilities of laumontite, wairakite, lawsonite, and related minerals in System $CaAl_2Si_2O_8$–SiO_2–H_2O. J Petrol 12: 379–411

Liou JG, Tsujimori T, Zhang RY, Katayama I, Maruyama S (2004) Global UHP metamorphism and continental subduction/collision: The Himalayan model. Int Geol Rev 46: 1–27

Maruyama S, Cho M, Liou JG (1986) Experimental investigations of blueschist-greenschist transition equilibrium: Pressure dependence of Al_2O_3 contents in sodic amphiboles – a new geobarometer. In: *Evans BW, Brown EH* (eds) Blueschist and Eclogites, Geol Soc Am Memoir 164, pp 1–16

Massonne HJ, Schreyer W (1987) Phengite geobarometry based on the limiting assemblage with K-feldspar, phlogopite, and quartz. Contrib Mineral Petrol 96: 212–224

Matsumoto M, Wallis S, Aoya M, Enami M, Kawano J, Seto Y, Shimobayashi N (2003) Petrological constraints on the formation conditions and retrograde P–T path of the Kotsu eclogite unit, central Shikoku. J Metamorph Geol 21: 363–376

Mattinson CG, Zhang RY, Tsujimori T, Liou JG (2004) Epidote-rich talc-kyanite-phengite eclogites, Sulu terrane, eastern China: P–T-$f(O_2)$ estimates and the significance of the epidote-talc assemblage in eclogite. Am Mineral 89: 1772–1783

Mattinson JM, Hopson CA (1992) U–Pb ages of the Coast Range ophiolite: a critical reevaluation based on new high-precision Pb–Pb ages. Am Assoc Petroleum Geol Bull 76: 425

Moore DE (1984) Metamorphic history of a high-grade blueschist exotic block from the Franciscan Complex, California. J Petrol 25: 126–150

Moore DE, Blake MC Jr (1989) New evidence for polyphase metamorphism of glaucophane schist and eclogite exotic blocks in the Franciscan Complex, California and Oregon. J Metamorph Geol 7: 211–228

Oh CW, Liou JG (1990) Metamorphic evolution of two different eclogites in the Franciscan Complex, California, U.S.A. Lithos 25: 41–53

Pattison DRM (2003) Petrogenetic significance of orthopyroxene-free garnet + clinopyroxene + plagioclase ± quartz-bearing metabasites with respect to the amphibolite and granulite facies. J Metamorph Geol 21: 21–34

Peacock SM, Wang K (1999) Seismic consequences of warm, versus cool subduction metamorphism: examples from Southwest and Northeast Japan. Nature 286: 937–939

Poli S, Schmidt MW (1997) The high-pressure stability of hydrous phases in orogenic belts: an experimental approach on eclogite-forming processes. Tectonophys 273: 169–184

Powell R, Holland TJB, Worley B (1998) Calculating phase diagrams involving solid solutions via non-linear equations, with examples using THERMOCALC. J Metamorph Geol 16: 577–588

Rad GRF, Droop GTR, Amini S, Moazzen M (2005) Eclogites and blueschists of the Sistan Suture Zone, eastern Iran: a comparison of P–T histories from a subduction melange. Lithos 84: 1–24

Ransome FL (1894) On lawsonite, a new rock forming mineral from the Tiburon Peninsula, Marin County, California. Univ California Dept Geol Sci Bull 1: 301–312

Ross JA, Sharp WD (1988) The effects of sub-blocking temperature metamorphism on the K/Ar systematics of hornblendes: $^{40}Ar/^{39}Ar$ dating of polymetamorphic garnet amphibolite from the Franciscan Complex, California. Contrib Mineral Petrol 100: 213–221

Saha A, Basu AR, Wakabayashi J, Wortman GL (2005) Geochemical evidence for a subducted infant arc in Franciscan high-grade-metamorphic tectonics blocks. Geol Soc Am Bull 117: 1318–1335

Schliestedt M (1990) Occurrences and stability conditions of low-temperature eclogites. In: *Carswell DA* (ed) Eclogite Facies Rocks, pp 160–179

Shervais JW (1990) Island arc and ocean crust ophiolites; contrasts in the petrology, geochemistry and tectonic style of ophiolite assemblages in the California Coast Ranges. In: *Malpas JC, Moores EM, Panayiotou A, Xenophontos C* (eds) Ophiolites, oceanic crustal analogues: Proceedings of the Symposium ''Troodos 1987'', Nicosia, Cyprus, Geol Surv Dept, Ministry of Agriculture and Natural Resources, pp 507–520

Shervais JW, Murchey BL, Kimbrough DL, Renne PR, Hanan B (2005) Radioisotopic and biostratigraphic age relations in the Coast Range Ophiolite, northern California:

Implications for the tectonic evolution of the Western Cordillera. Geol Soc Am Bull 117: 633–653

Shibakusa H, Maekawa H (1997) Lawsonite-bearing eclogitic metabasites in the Cazadero area, northern California. Mineral Petrol 61: 163–180

Tropper P, Manning CE (2004) Paragonite stability at 700 °C in the presence of H_2O–NaCl fluids: constraints on H_2O activity and implications for high-pressure metamorphism. Contrib Mineral Petrol 147: 740–749

Tsujimori T (2002) Prograde and retrograde P–T paths of the Late Paleozoic glaucophane eclogite from the Renge metamorphic belt, Hida Mountains, Southwestern Japan. Int Geol Rev 44: 797–818

Tsujimori T, Ishiwatari A (2002) Granulite facies relics in the early Paleozoic kyanite-bearing ultrabasic metacumulate in the Oeyama belt, the inner zone of southwestern Japan. Gondwana Res 5: 823–835

Tsujimori T, Itaya T (1999) Blueschist-facies metamorphism during Paleozoic orogeny in southwestern Japan: phengite K–Ar ages of blueschist-facies tectonic blocks in a serpentinite melange beneath Early Paleozoic Oeyama ophiolite. Island Arc 8: 190–205

Tsujimori T, Liou JG (2004a) Coexisting chromian omphacite and diopside in tremolite schist from the Chugoku Mountains, SW Japan: The effect of Cr on the omphacite-diopside immiscibility gap. Am Mineral 89: 7–14

Tsujimori T, Liou JG (2004b) Metamorphic evolution of kyanite-staurolite-bearing epidote-amphibolite from the Early Paleozoic Oeyama belt, SW Japan. J Metamorph Geol 22: 301–313

Tsujimori T, Liou JG (2005) Eclogite-facies mineral inclusions in clinozoisite from Paleozoic blueschist, central Chugoku Mountains, southwest Japan: Evidence of regional eclogite-facies metamorphism. Int Geol Rev 47: 215–232

Tsujimori T, Liou JG, Coleman RG (2005) Coexisting retrograde jadeite and omphacite in a jadeite-bearing lawsonite eclogite from the Motagua fault zone, Guatemala. Am Mineral 90: 836–842

Tsujimori T, Liou JG, Coleman RG (2006) Finding of high-grade tectonic blocks from the New Idria serpentinite body, Diablo Range, California: Petrologic constraints on the tectonic evolution of an active serpentinite diapir. In: *Cloos M, Carlson WD, Gilbert MC, Liou JG, Sorensen SS* (eds) Convergent Margin Terranes and Associated Regions – a tribute to *W. G. Ernst*, Geol Soc Am Spec Paper

Tsujimori T, Matsumoto K (2006) P–T pseudosection of a glaucophane-epidote eclogite from Omi serpentinite melange, SW Japan: a preliminary report. J Geol Soc Japan 112: 407–414

Wakabayashi J (1987) Amphibolite grade metamorphism of Franciscan rocks from the San Francisco Bay Area, California. Geol Soc Am Abst Program 19: 460

Wakabayashi J (1990) Counterclockwise P–T-t paths from amphibolites, Franciscan Complex, California: Metamorphism during the early stages of subduction. J Geol 98: 657–680

Wakabayashi J (1992) Nappes, tectonics of oblique plate convergence, and metamorphic evolution related to 140 million years of continuous subduction, Franciscan Complex, California. J Geol 100: 19–40

Wakabayashi J (1999) Subduction and the rock record: Concepts developed in the Franciscan Complex, California. Geol Soc Am Spec Paper 338: 123–133

Wakabayashi J, Dilek Y (2003) What constitutes ''emplacement'' of an ophiolite?: mechanisms and relationship to subduction initiation and formation of metamorphic soles. In: *Dilek Y, Robinson PT* (eds) Ophiolites in Earth history, Geol Soc London Spec Publ 218, pp 427–447

Waters D, Martin HN (1993) The garnet-clinopyroxene-phengite barometer. Terra Abst 5: 410–411

Wei C, Powell R, Zhang LF (2003) Eclogites from the south Tianshan, NW China: petrological characteristic and calculated mineral equilibria in the Na_2O–CaO–FeO–MgO–Al_2O_3–SiO_2–H_2O system. J Metamorph Geol 21: 163–179

Will TM, Okrusch M, Schmädicke E, Chen G (1998) Phase relations in the greenschist-blueschist-amphibolite-eclogite facies in the system Na_2O–CaO–FeO–MgO–Al_2O_3–SiO_2–H_2O (NCFMASH), with applications to the P–T-evolution of metamorphic rocks from Samos, Greece. Contrib Mineral Petrol 132: 85–102

Zhang RY, Liou JG, Tsujimori T, Maruyama S (2006) Non-UHP unit bordering the Sulu UHP terrane, eastern China: Transformation of Proterozoic granulite and gabbro to garnet amphibolite. In: *Hacker BR, McClelland W, Liou JG* (eds) Ultrahigh-Pressure Metamorphism: Deep Continental Subduction. Geol Soc Am Spec Paper, pp 169–207

Author's present address: *Tatsuki Tsujimori*, Venture Business Laboratory, Kanazawa University, Kanazawa 920-1192, Japan, e-mail: tatsukix@mac.com